Braz J Phys (2013) 43:22–27
DOI 10.1007/s13538-012-0109-7

SOCIEDADE BRASILEIRA DE FÍSICA

CONDENSED MATTER

Magnetic Measurements and Kinetic Energy of the Superconducting Condensate in $SmBa_2Cu_3O_{7-\delta}$

J. P. Peña · D. B. Martínez · C. A. Parra Vargas · A. G. Cunha · J. L. Pimentel Jr. · P. Pureur

Received: 16 January 2012 / Published online: 28 November 2012

Abstract We report in-field kinetic energy results in the temperature region closely below the transition temperature of two differently prepared polycrystalline samples of the superconducting cuprate $SmBa_2Cu_3O_{7-\delta}$. The kinetic energy is determined from magnetization measurements performed above the irreversibility line defined by the splitting between the curves obtained according the zero field cooling and field cooling prescriptions. The results are analyzed in the intermediate field regime, where the London approximation can be used to describe the magnetization. From the analysis, estimations are obtained for the penetration depth and the upper critical field of the studied samples. The difference between the magnitudes of the kinetic energy in the two studied samples is ascribed to granularity effects.

Keywords Kinetic energy density · Vortex lattice · Granularity

J. P. Peña · D. B. Martínez · C. A. Parra Vargas
Grupo de Física de Materiales, Universidad Pedagógica y Tecnológica de Colombia, Av. Central del Norte, Tunja, Colombia

J. P. Peña (✉) · J. L. Pimentel Jr. · P. Pureur
Instituto de Física, Universidade Federal do Rio Grande do Sul, Av. Bento Gonçalves 9500, C.P. 15051, 91501-970, Porto Alegre, Rio Grande do Sul, Brazil
e-mail: jullypaola@if.ufrgs.br

A. G. Cunha
Departamento de Física, Universidade Federal do Espírito Santo, Av. Fernando Ferrari 514, Campus Goiabeiras, 29075-910, Vitória, Espírito Santo, Brazil

1 Introduction

The experimental study of the kinetic energy of the charge carriers in the high-temperature cuprate superconductors (HTCS) has become an important subject in view of the new theoretical approaches predicting that, in the absence of an applied magnetic field, pairing in these materials results from a decrease of the kinetic energy term upon condensation [1, 2]. This prediction is opposite to that of the Bardeen–Cooper–Schrieffer (BCS) theory, in which the kinetic energy of the carriers increases when the system enters the superconducting state [3].

Experimentally, the situation is less clear because the change of the kinetic energy in the condensate with respect to that of the normal state is relatively small. The spectral-weight transfer observed below the superconducting transition in optical conductivity measurements in optimally doped and underdoped $Bi_2Sr_2CaCu_2O_{8+d}$ (Bi-2212) favors the unconventional scenario of decreasing kinetic energy [4]. On the other hand, when this cuprate is slightly overdoped, the results are rather in accordance with the BCS predictions [5].

A simpler situation occurs in a type-II superconductor when a magnetic field is applied. In that case, the kinetic energy of the condensate is expected to always increase because of flux expulsion and vortex formation [6]. Useful informations may be obtained on the order parameter and other basic properties of type-II superconductors from studies of this energy term [7]. In the case discussed here, we are interested in the kinetic energy associated with the currents around the vortices generated by the action of an applied external magnetic field.

Theoretically, it was demonstrated from an application of the virial theorem in the framework of the Ginzburg–Landau (G–L) theory [8] that the average kinetic energy density of a large κ superconductor may be written in the form [6, 7]

$$E_K = -\vec{M} \cdot \vec{B}\,, \tag{1}$$

where $\vec{M}$ is the equilibrium magnetization and $\vec{B}$ is the magnetic induction. Inside a superconducting sample, the induction (in the SI system) may be written as $\vec{B} = \mu_0 \vec{H} + \mu_0(1+\eta)\vec{M}$, where μ_0 is the vacuum permeability, $\vec{H}$ is the applied field, and η is the sample-dependent geometric factor related to the dipolar field. Then, to obtain the kinetic energy density from magnetization measurements, it is useful to rewrite (1) as

$$E_K = -\mu_0 \vec{M} \cdot \vec{H} - \mu_0(1+\eta)\, M^2. \tag{2}$$

The in-field kinetic energy density was determined for a few low and high T_c superconductors in Refs. [6, 9] and [10]. The reported results for Nb [9] and for a Pb-In alloy [10] agree with the expectations derived from the Abrikosov treatment of the G–L theory, as well as with general BCS predictions. On the other hand, in such cuprates as optimally doped and underdoped $YBa_2Cu_3O_x$ (YBCO) [9], optimally doped Bi-2212 [9], and $La_{1.9}Sr_{0.1}CuO_4$ [10], an appreciable amount of the in-field kinetic energy subsists up to temperatures well beyond T_c. The authors of Refs. [9] and [10] identify this behavior with a pseudogap effect, although the influence of strong thermal fluctuations cannot be ruled out as an alternative explanation.

In order to study the differences induced in the kinetic energy by the microscopic morphology, we report here magnetization measurements and in-field kinetic energy density estimations in two different polycrystalline samples of $SmBa_2Cu_3O_{7-\delta}$ (Sm-123). The experiments were performed in several applied fields. However, the extraction of $E_K(T, H)$ is restricted to the temperature range near T_c, where the equilibrium magnetization can be unambiguously obtained from coincident and reproducible ZFC and FC measurements. Results are compared to those obtained in YBCO and Bi-2212 single crystals [9, 10]. The magnitude of the kinetic energy of our polycrystalline samples is considerably smaller than that of single crystal samples.

2 Experimental

Two samples of polycrystalline $SmBa_2Cu_3O_{7-\delta}$ (Sm-123) were independently produced using the solid-state reaction method. The employed procedures are described below. The precursor compounds Sm_2O_3 (purity 99.99 %), $BaCO_3$ (purity 99.8 %), and CuO (purity 99.995 %) were used to prepare the samples. For the sample labeled Sm-I, the precursors were mixed and macerated during 2 h in an agate mortar, pressed at 3 tons into a cylindrical shape and submitted to a calcination process at 850 °C during 15 h. After furnace cooling to room temperature, the resulting pellet was finely powdered again, pressed and subjected to two sintering processes at 870 and 890 °C for 45 h each. The cylindrical sample was then oxygenated by exposure to an oxygen atmosphere while decreasing the temperature in the range of 750–250 °C at a rate of 12.5 °C/h, then it was furnace-cooled to room temperature.

Sample Sm-II was also prepared in three steps, but different equipments and thermal processes were used. In the calcination process, the macerated and pressed precursors were heated up to 850 °C and kept at this temperature during 48 h. For the sintering step, the sample was heated up to 900 °C at 150 °C/h, kept at this temperature for 0.1 h, then heated up to 1,040 °C at 60 °C/h. After a 24-h annealing at this temperature, the sample was cooled at −60 °C/h to 900 °C, at which temperature it was kept for 0.1 h. Subsequently, the sample was cooled down to room temperature at 150 °C/h. In the final oxygenation process, the sample Sm-II was heated again to 500 °C and kept at this temperature during 0.1 h. Then, it was cooled to 350 °C and kept at this temperature for 3 days. After that time, it was furnace-cooled to room temperature.

Electrical resistivity measurements were performed in both samples. Transition temperatures determined from the maximum of the temperature derivative of the resistivity are $T_c = 92.7$ K for sample Sm-I and $T_c = 89.9$ K for sample Sm-II. The width of the resistive transition is around 3 K for both samples.

Zero field cooling (ZFC) and field cooling (FC) magnetization measurements in several applied fields ranging from 1 mT up to 5 T were performed using a XL5-MPMS SQUID magnetometer manufactured by Quantum Design Inc. Results were corrected for demagnetization effects. The geometrical factors were estimated on the basis of the calculations in Ref. [11], the shapes of the samples approximated by ellipsoids. The porosity of the ceramic samples was also taken into account by comparing the measured densities to the theoretically expected values.

3 Results

3.1 Reversible Magnetization and Fluctuation Effects

Figure 1 shows representative magnetization versus temperature results in a temperature range encompassing the superconducting transition for the two studied samples. Results for samples Sm-I and Sm-II are shown in panels a and b, respectively. The experiments were performed according the ZFC and FC prescriptions. The irreversibility temperature $T_{\rm irr}$ denotes the point below which pinning effects become important. We carried out our analyses in the temperature regime above $T_{\rm irr}$, in which the experimental data describe the equilibrium magnetization with no ambiguity. The extension of the magnetically reversible regime in high applied fields is smaller for sample Sm-II than for sample Sm-I.

Figures 2a, b collect the characteristic temperatures T_c and $T_{\rm irr}$ for samples Sm-I and Sm-II, respectively, in several applied fields. The area delimited between the curves $T_c(H)$ and $T_{\rm irr}(H)$ defines the reversible region, where the effects of the pinning energy are negligible. The field-dependent critical temperatures are determined by the intersection between the linearly extrapolated magnetizations in the normal and superconducting phases, as illustrated by the inset of Fig. 1a. The irreversibility temperatures are determined by subtracting the ZFC magnetization from the FC one and applying the criterion in Ref. [12]: $T_{\rm irr}(H)$ is the temperature at which the difference $M_{\rm FC}(T, H) - M_{\rm ZFC}(T, H)$ deviates from the zero baseline defined by the high-temperature data.

The observed behavior of $T_{\rm irr}(H)$ for the two samples is typical of polycrystalline samples of HTCS [13] and mimics observations in spin glass systems. For sample Sm-I, in the low-field, high-temperature limit, the irreversibility temperatures decrease as a function of the applied field as $[T_{\rm irr}(0) - T_{\rm irr}(H)] \sim H^{2/3}$, in analogy to the de Almeida–Thouless line [14]. As shown in Fig. 2a, near $\mu_0 H = 0.5$ T, a crossover is observed in $T_{\rm irr}(H)$ to an inverse curvature field dependence that is approximately fitted by a Gabay–Toulouse-like line [15], given by $[T_{\rm irr}(0) - T_{\rm irr}(H)] \sim H^2$. The behavior of the filled squares in Fig. 2a is analogous to the crossover from the high-field Gabay–Toulouse transition to the low-field de Almeida-Thouless instability observed in Heisenberg vector spin glasses [16]. As shown by Fig. 2b, a de Almeida–Thouless-like line describes the irreversibility line for sample Sm-II over the entire field range. These results suggest that granularity effects are stronger in sample Sm-I.

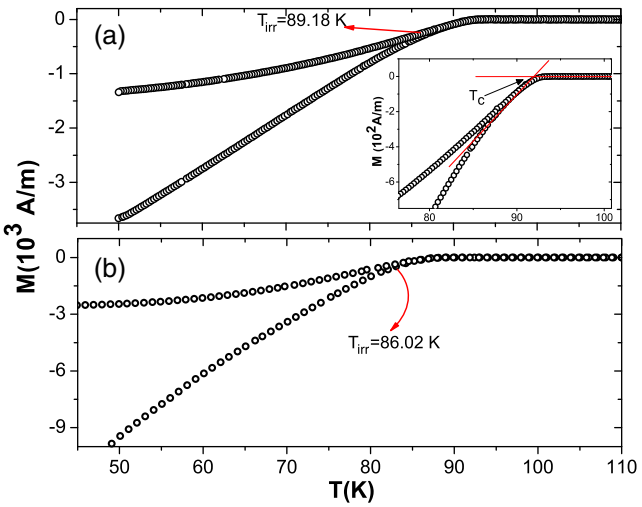

Fig. 1 Zero field cooled and field cooled magnetizations as functions of the temperature for polycrystalline $SmBa_2Cu_3O_{7-\delta}$ (Sm-123) measured at $\mu_0 H = 0.05$ T. **a** Results for sample Sm-I (see text). The *inset* illustrates the criterion used to define the in-field critical temperatures. **b** Results for sample Sm-II. In each panel, the indicated irreversibility temperatures $T_{\rm irr}$ signals the splitting of the ZFC and FC curves. Corrections for the demagnetizing field effects are taken into account

3.2 Kinetic Energy

We assume that the G–L theory describes the equilibrium magnetization adequately in most of the reversible superconducting regime of our samples. Then, using the prescription of Doria et al. [6], we plot in Figs. 3a, b the field-induced kinetic energy given by (2) as a function of temperature for samples Sm-I and Sm-II, respectively. Results for magnetic fields ranging from 0.2 up to 5 T are shown, and the data are restricted to the temperature regime in which the magnetization is reversible. The applied field range in our investigation significantly enlarges the regime studied in Ref. [9] for YBCO. Here, the kinetic energy density approaches the temperature axis linearly and vanishes for $T \approx T_c(H)$. In contrast with the findings reported in Ref. [9], we do not observe a significant kinetic energy contribution above T_c. On the other hand, the kinetic energies E_K in Sm-123 and YBCO are qualitatively similar in the field and temperature range where comparison is possible, even though the YBCO results were obtained for fields applied perpendicular to the Cu-O_2 atomic layers of a single crystal sample [9].

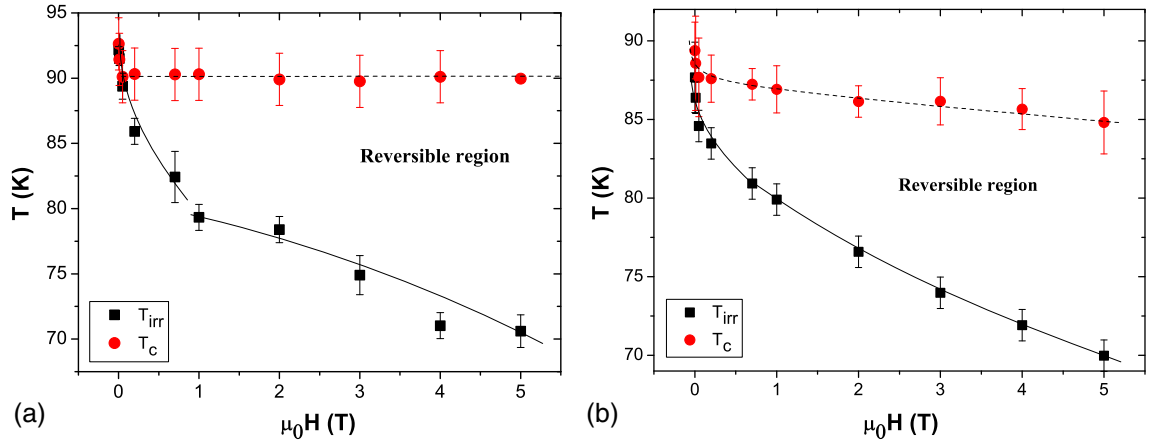

Fig. 2 Critical temperatures and irreversibility temperatures as functions of the applied field for samples Sm-I **a** e Sm-II **b**. The *solid* and the *dashed lines* are guides to the eye

Notwithstanding the qualitative similarities between the field and temperature behaviors in Figs. 3a, b, the data for samples Sm-I and Sm-II differ quantitatively. For a given field and temperature, E_K is significantly larger for sample Sm-II. We attribute this difference to polycrystallinity. Indeed, the different routes employed to prepare our samples are likely to yield distinct granular microstructures, and granularity is known to affect the magnetic behavior of polycrystalline samples of the HTCS.

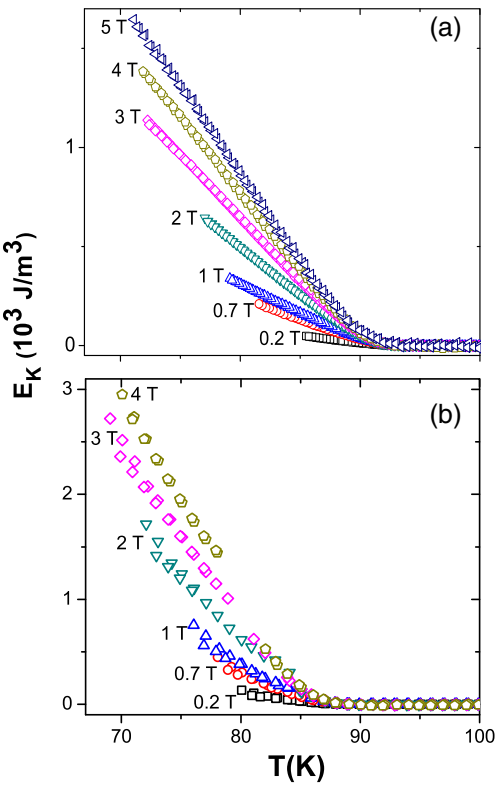

Fig. 3 Kinetic energy density as a function of the temperature for samples **a** Sm-I and **b** Sm-II in the indicated applied fields

In the intermediate field regime, $H_{c1} \ll H \ll H_{c2}$, the interaction among the vortices is weak [3]. In this field region, the Cooper pair density may be considered uniform inside the sample excepting the vortex positions. In the case of extreme type-II superconductors ($\kappa >> 1$), such as the HTCS, the variation of the order parameter in the vortex positions can be described by delta functions. Under such conditions, the magnetization can be calculated with the London approximation to the G–L theory. In this case, the magnetization in SI units is given by the expression [17]:

$$M(H) = -\frac{\phi_0}{8\mu_0\pi\lambda^2}\ln\left(\frac{\beta_L H_{c2}}{H}\right), \tag{3}$$

where ϕ_0 is the quantum magnetic flux, μ_0 is the vacuum permeability, λ is the penetration length, and β_L is a constant of the order of unity.

Substitution of the magnetization given by (3) in (2) yields the expression

$$\frac{E_K(\mu_0 H)}{\mu_0 H} = \frac{\phi_0}{8\pi\lambda^2\mu_0}\ln\frac{\beta_L\mu_0 H_{c2}}{\mu_0 H} - \left(\frac{\phi_0}{8\pi\lambda^2}\right)^2\frac{1}{\mu_0^2 H}\left(\ln\frac{\beta_L\mu_0 H_{c2}}{\mu_0 H}\right)^2. \tag{4}$$

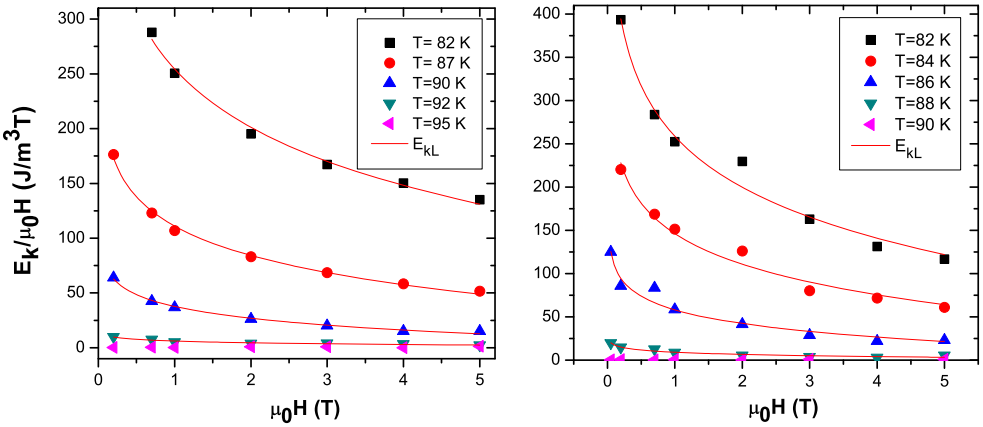

Fig. 4 Kinetic energy per field unit for samples Sm-I (*left*) and Sm-II (*right*). The *solid lines* are fits of (4) to the experimental data

Figure 4 displays fits of (4) to the experimental data for samples Sm-I and Sm-II. From these fits, we estimate the penetration lengths and the upper critical field in the studied field and temperature ranges[1]. The resulting $\lambda(T)$ and $H_{c2}(T)$ were corrected according to the Hao and Clem model [18] and are shown in Figs. 5 and 6, respectively.

According to mean-field theory, $\lambda(T) = \frac{1}{\sqrt{2}}\lambda(0)t^{-1/2}$ and $B_{c2}(T) = 1,83\,B_{c2}(0)t$ where $t = (T_c - T)/T_c$ is the reduced temperature [19]. In Fig. 5, $\lambda(T)$ is plotted as a function of $1/\sqrt{t}$ for samples Sm-I and Sm-II . The fitted straight lines allow us to estimate $\lambda(0) = 516 \pm 12$ nm for sample Sm-I and $\lambda(0) = 363 \pm 7$nm for sample Sm-II. These values are within the expected range, since the estimated penetration lengths are polycrystalline averages enhanced by granularity effects [20]. The larger $\lambda(0)$ for sample Sm-I also suggests that the influence of granularity is stronger in this sample.

In Fig. 6, the estimations for H_{c2} extracted from the fittings in Fig. 4 are plotted as a function of the reduced temperature. The data for both samples align in a single straight line. From the slope of line, we deduce that $B_{c2}(0) = 130$ T for Sm-123. This estimation is in good agreement with previous determinations of polycrystalline averages of the upper critically induced field in Y-123-type superconductors [19].

Since granularity makes polycrystalline HTCS systems behave as a superconducting glassy medium [21], the in-field kinetic energy in our Sm-123 samples may not be entirely accounted by the London approximation to the Ginzburg–Landau theory. A complete description of the kinetic energy in granular HTCS should include the contributions of Josephson vortices [22] and intergrain chiralities [23]. As a first approximation, however, (4) offers a good description of the data, showing that the intragrain vortices are indeed the dominant contribution to the condensate kinetic

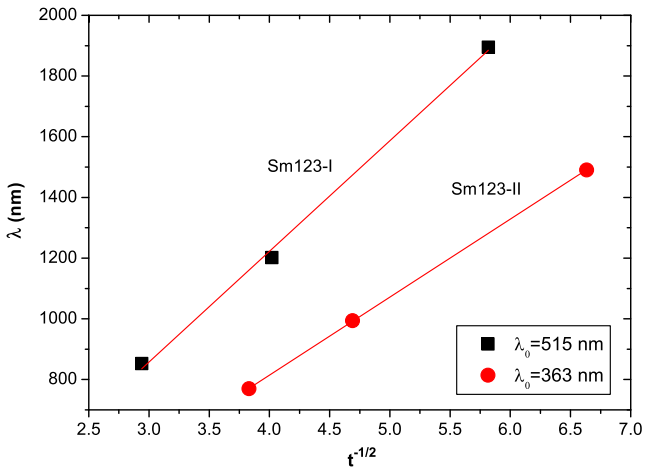

Fig. 5 Penetration lengths as functions of $1/\sqrt{t}$ for samples Sm-I and Sm-II, deduced from the fits of (4) to the experimental data in Fig. 4

[1]The penetration length and the upper critical field could be estimated directly from equation (3) and measurements of the magnetization in various magnetic fields. Since we are centrally interested in the kinetic energy, however, we find it more instructive to work all of this in the frame of the E_K obtained by applying (4) (solid lines in Fig. 4) which allows to verify that the employed theory leads to good results.

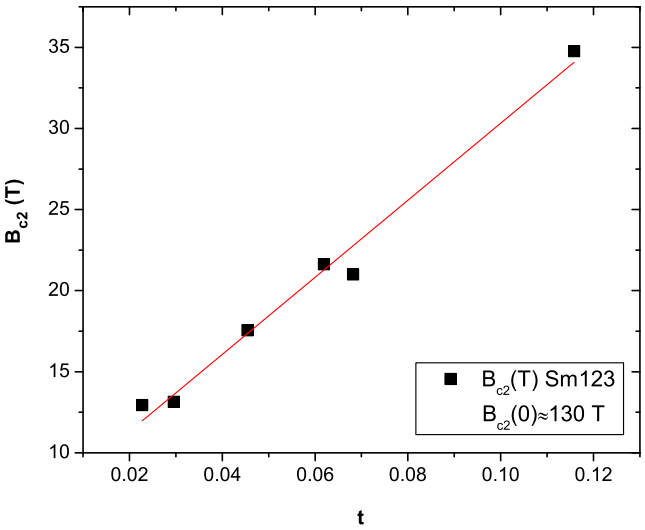

Fig. 6 Upper critical field for samples Sm-I and Sm-II as deduced from the results in Fig. 4. Data points are plotted as a function of the reduced temperature. A *single straight line* fits the data for both samples

energy in Sm-123 in the investigated field temperature range.

4 Conclusions

We studied the reversible magnetization and the field-induced kinetic energy density in two polycrystalline samples of the $SmBa_2Cu_3O_{7-\delta}$ cuprate superconductor experimentally. Our analysis was restricted to the temperature range nearly below T_c, where the ZFC and FC magnetization are coincident. Fields up to 5 T were applied.

The theory proposed by M. Doria and co-workers [6, 7], based on the application of the virial theorem to the Ginzburg–Landau free energy, was used to describe the kinetic energy density in our samples. The magnitude of the kinetic energy was found to be larger for sample Sm-II than for sample Sm-I, a difference pointing to more enhanced granularity effects in the latter. The identified contribution to the kinetic energy in both samples were attributed to intragrain vortices. The results were interpreted on the basis of the London approximation to the Ginzburg–Landau theory. The penetration length and the upper critical field were calculated for both samples. The obtained values are similar to those found in previous studies. The penetration length estimations corroborate the conclusion that granularity effects are more enhanced in sample Sm-I.

As a final conclusion, our results and analyses showed that the study of the in-field kinetic energy may improve the usual description of the magnetic response of superconductors based solely on magnetization measurements in the temperature range approaching T_c, where pinning effects are absent.

Acknowledgements We thank Dr. Mauro Doria for enlightening discussions on the in-field kinetic energy of a superconducting condensate. This work was partially financed by the Brazilian agencies FAPERGS and CNPq under the grant PRONEX 10/0009-2.

References

1. V.J. Emery, G. Reiter, Phys. Rev. B **38**, 4547 (1988)
2. J.E. Hirsch, Physica C **201**, 347 (1992)
3. M. Tinkham, *Introduction to Superconductivity* (Krieger, Malabar, 1975)
4. H.J.A. Molegraaf, C. Presura, D. van der Marel, P.H. Kes, M. Li, Science **295**, 2239 (2002)
5. G. Deutscher, A.F. Santander-Syro, N. Bontemps, Phys. Rev. B **72**, 092504 (2005)
6. M.M. Doria, S. Salem-Sughi Jr., I.G. de Oliveira, L. Ghivelder, E.H. Brandt, Phys. Rev. B **65**, 144509 (2002)
7. M.M. Doria, J. Supercond. Nov. Magn. **22**, 235 (2009)
8. M.M. Doria, J.E. Gubernatis, D. Rainer, Phys. Rev. B **39**, 9573 (1989)
9. S. Salem-Sugui Jr., M.M. Doria, A.D. Alvarenga, V.N. Vieira, P.F. Farinas, J.P. Sinnecker, Phys. Rev. B **76**, 132502 (2007)
10. M.M. Doria, S. Salem-Sugui Jr. Phys. Rev. B **78**, 134527 (2008)
11. J.A. Osborn, Phys. Rev. **67**, 351 (1945).
12. F.T. Dias, V.N. Vieira, P. Rodrigues Jr., X. Obradors, P. Pureur, J. Schaf, Phys. Rev. B **77**, 134503 (2008)
13. P. Rodrigues Jr., J. Schaf, P. Pureur, Phys. Rev. B **49**, 15292 (1994)
14. J.R.L. de Almeida, D.J. Thouless, J. Phys. A **11**, 983 (1978)
15. M. Gabay, G. Toulouse, Phys. Rev. Lett. **47**, 201 (1981)
16. N. de Courtenay, A. Fert, I.A. Campbell, Phys. Rev. B 30, 6791 (1984).
17. P.G. de Gennes, *Superconductivity of metals and alloys* (Addison Wesley Publishing Co., 1989)
18. Z. Hao, J.R. Clem, Phys. Rev. Lett. **67**, 2371 (1991)
19. M. Cyrot, D. Pavuna, *Introduction to Superconductivity and high Tc materials* (World Scientific Publications, Co.Pte.Ltd, 1992)
20. K.A. Muller, M. Takashige, J.G. Bednorz, Phys. Rev. Lett. **58**, 1143 (1987)
21. V.N. Vieira, J. Schaf, Phys. Rev. B **65**, 144531 (2002)
22. H. Kawamura, M.S. Li, J. Phys. Soc. Jpn. **66**, 2110 (1997)
23. G. Blatter, M.V. Feigel'man, V.B. Geshkenbein, A.I. Larkin, V.M. Vinokur, Rev. Mod. Phys. **66**, 1125 (1994)